Simulation of Hybrid Trickle Bed Reactor-Reverse Osmosis Process for the Removal of Phenol from Wastewater

M. A. Al-Obaidi [a, b], A. T. Jarullah [c], C. Kara-Zaïtri [a] and I. M. Mujtaba [a, *]

[a] Chemical Engineering Division, School of Engineering, University of Bradford, Bradford, West Yorkshire BD7 1DP, UK

[b] Middle Technical University, Baghdad – Iraq

[c] Chemical Engineering Department, College of Engineering, Tikrit University, Iraq

***Corresponding author, Tel.: +44 0 1274 233645**

E-mail address: I.M.Mujtaba@bradford.ac.uk

Abstract

Phenol and phenolic derivatives found in different industrial effluents are highly toxic and extremely harmful to human and the aquatic ecosystem. In the past, trickle bed reactor (TBR), reverse osmosis (RO) and other processes have been used to remove phenol from wastewater. However, each of these technologies has limitations in terms of the phenol concentration in the feed water and the efficiency of phenol rejection rate. In this work, an integrated hybrid TBR-RO process for removing high concentration phenol from wastewater is suggested and model-based simulation of the process is presented to evaluate the performance of the process. The models for both TBR and RO processes were independently validated against experimental data from the literature before coupling together to make the hybrid process. The results clearly show that the combined process significantly improves the rejection rate of phenol compared to that obtained via the individual processes.

***Keywords*:** Wastewater Treatment; Integrated Process: Trickle bed Reactor: Reverse Osmosis (RO); Phenol Rejection; Modelling.

1. Introduction

Wastewater effluents of many industrial processes contain a variety of micro-pollutants which are released into the environment. These pose a real threat to the water supply for human consumption and to the aquatic ecosystems (Pomiès *et al.*, 2013). The most common and indeed the most harmful micro-pollutants are the phenols (Busca *et al.*, 2008; Mohammed *et al.*, 2016), which are present in wastewater of different industries including;

- Refineries (6-500 ppm).
- Cooking process (27-3900 ppm).
- Coal processing (9-6800 ppm).
- Manufacture of petrochemical (28-1220 ppm).
- Pharmaceutical, wood products, paint and pulp (0.1-1600 ppm).

Phenols are particularly harmful because of their high toxicity even at low concentration (Ahmed *et al*., 2010). For example, dose of only 140 mg/kg bw of phenol in humans is lethal (Bingham *et al*., 2001). The European Food Standards Agency (EFSA) recently established the oral tolerable daily intake TDI to be at 0.5 mg/kg/day for phenol (EFSA, 2013). Thus, the removal of phenol from aqueous solutions has received much attention and has resulted in a wide range of treatment methods (Mohammadi *et al*., 2015) such as (a) Separation by adsorption using granular and powdered activated carbon, especially for diluted aqueous solutions (b) Electrochemical oxidation (chlorine and hypochlorite) (c) Photo oxidation processes where phenol oxidation activity is under the UV irradiation (d) Oxidation with chemical oxidants (O_3 ozonation and H_2O_2). .

In addition to the above processes, most recently Mohammed *et al.* (2016) considered the catalytic wet air oxidation (CWAO) process using a trickle bed reactor (TBR) for the removal of phenol from wastewater.

Also, Reverse Osmosis (RO) process has been used by several authors for the removal of phenol and phenolic compounds from wastewater (Srinivasan et al., 2010; Sundaramoorthy *et al*.,2011; Al-Obaidi *et al*.,2017b).

In the open literature there are also references to the use of a number of hybrid processes. Geraldes *et al*. (2008) have used a coagulation/flocculation step and a bench-scale dissolved air flotation (DAF) of Tagus River surface water (Valadas, Portugal) as a pre-treatment process for a spiral wound module nanofiltration to remove colloidal matter and suspended solids. The resulting experimental data confirmed that the hybrid process has in fact modified the silt density index and fouling index of the treated water, which are used to measure the concentration of pollutants. Also, Sudilovskiy *et al.* (2008) have integrated the membrane flotation process (microporous ceramic membranes are used as air diffusers) and commercial spiral wound RO and NF membrane modules for the treatmentof wastewaters containing copper and other heavy metals. This proposed hybrid system has resulted in a high rejection of the harmful compounds

and high pure water recovery. Al-Zoubi *et al.* (2009) suggested a hybrid dissolved air flotation (DAF)-membrane process for the treatment of many types of wastewater. Kim *et al*. (2009) investigated the hybrid system of granular activated carbon (GAC) and MF membrane in terms of both quality (dissolved organic carbon) and quantity (permeate flux) for water purification and wastewater reclamation/reuse. This study confirmed that the hybrid process is more effective in wastewater treatment than the MF membrane process.

Hybrid processes have been proposed in the literature for seawater and wastewater treatment problems yielding a number of advantages, including; enhanced quality of water, reduced cost of production, energy saving and environmental compliance (Ang *et al*., 2015; Altaee and Hilal, 2015).

More recently, Mozia *et al.* (2016) evaluated the hybrid system in a pilot-scale experiment by using the bed biofilm reactor (HMBBR), an UV/O_3 advanced oxidation (photoreactor) and UF and NF membrane units for the treatment and reuse of wastewater from an industrial laundry. The study showed that the integrated process resulted in high removal rates of organic contaminants of the laundry wastewater. Also, Pimple *et al*. (2016) implemented the combination of UF, membrane bioreactor (MBR) and RO processes for the removal of highly toxic compounds of cyanides and phenols from the coke-oven wastewater in order to produce an effluent that is fit for recirculation and horticultural practices. This study concluded that the hybrid system of UF/MBR-RO offers a high rejection rate of cyanides and phenols by about 90 ± 2% and 95 ± 3% respectively.

To the best of authors' knowledge, the implementation of integrated hybrid process combining the TBR and RO processes have not been considered yet. Therefore, the focus of this paper is to evaluate the performance of such process using modelling and simulation.

2. Description of the Hybrid Trickle Bed Reactor (TBR) – Reverse Osmosis (RO) Process

The catalytic wet air oxidation CWAO process is becoming prevalent in the treatment of various industrial toxic and persistent wastes. This process is based on the oxidation of organic matter in an aqueous phase using oxygen at the operating conditions of 100–350 °C and 4.93 to 197.38 atm of reaction temperature and pressure respectively (Gogate and Pandit, 2004; Safaa, 2009; Mohammed *et al.*, 2016). Reverse osmosis (RO), on the other hand, has been widely used for wastewater treatment but more specifically for the treatment of low concentration and low

molecular weight organic compounds. The use of RO to remove organic and non-organic pollutants have been analysed by several researchers including Ozaki H. and Li, 2002; Frederik Schutte, 2003; Hidalgo *et al*., 2011; Alzahrani*et al*., 2013a,b; Srinivasan et al., 2010; Sundaramoorthy *et al*., 2011).

The above two processes are combined together to provide the hybrid process as shown in Fig. 1. The individual processes are described in detail in the original references (Safaa, 2009; Mohammed *et al.*, 2016; Srinivasan et al., 2010; Sundaramoorthy *et al.*, 2011) but are summarised below for the convenience of the readers.

The TBR process comprises of fixed bed of a catalyst where wastewater is pumped from a feed tank under different operating conditions of initial phenol concentrations, oxygen partial pressure, reaction temperature, liquid hourly space velocity and gas flow rate. Compressed Pure O_2 from an oxygen cylinder is then fed co-currently with the feed wastewater stream into the reactor. The oxidization reaction is carried out inside the reactor between phenol and oxygen with a solid catalyst along the reactor.

For the hybrid process, it is very important to cool down the hot outlet reactor stream to the desired temperature of the RO process (~35 C) and also to separate any remaining gas using a separator. Therefore, a heat exchanger and a gas-liquid separator are used in between the two processes (Fig. 1). The wastewater liquid from the separator is then fed to the reverse osmosis RO process via a high-pressure pump capable of increasing the pressure up to 20 atm.

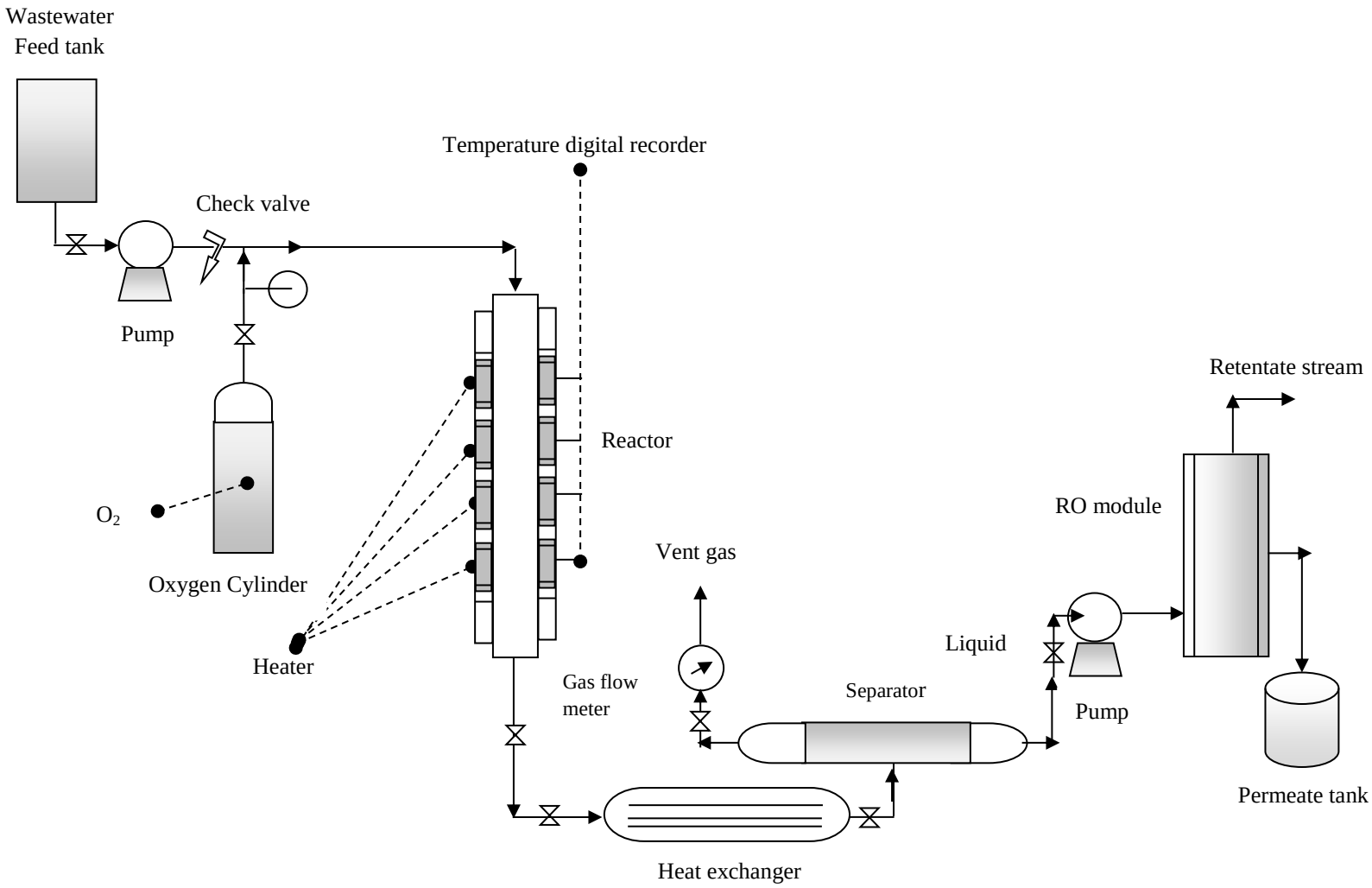

Fig. 1. Schematic diagram of the hybrid system of TBR-RO

3. Model for the Hybrid Process

3.1 Tickle Bed Reactor (TBR)

Modelling any process requires the determination of optimal operating conditions for testing several design alternatives during simulation and validation for improved efficiency. In this work, we used the model developed by Mohammed *et al*. (2016), which is a one-dimensional mathematical model based on Langmuir-Hinshelwood formulation to estimate the performance of a TBR used for the oxidation of phenol in wastewater effluents using pure oxygen and catalyst ($Pt/\gamma–Al_2O_3$). This proposed model consisted of a set of ordinary algebraic and differential equations related to mass and energy balance in addition to the physical properties equations. The model has been used by Mohammed *et al*. (2016) to simulate the TBR process. The model is shown in a more detail in Appendix A, Table A.1 for the convenience of the reader.

3.2 Spiral-wound Reverse Osmosis Process (SWRO)

Al-Obaidi *et al.* (2017b) developed a one-dimensional SWRO model for the removal of chlorophenol. In this work, we modified their model by incorporating thermophysical properties related to phenol. The model characterises the variation of operating parameters along the x-axis and estimate the rejection of phenol from its aqueous solutions. The reference equations used in this model are given in Appendix A, Table A.2 for the convenience of the reader.

3.3 Estimation of Unknown Model Parameters

Unknown parameters of any mathematical model and the operating conditions are normally determined before solving the associated equations. The gPROMS software (Process System Enterprise Ltd, 2001) provides a good tool for parameter estimation (*gEST*) which is based on minimum errors between the experimental data and the predicted data of the model. Also, the gPROMS software provides two approaches for modeling the optimization problem into a Linear Regression Programming (*LRP*) and Non-Linear Programming (*NLP*) problems. Both can be solved using a Successive Quadratic Programming (*SQP*) method available in the software suite.

3.3.1 TBR Process

Mohammed *et al.* (2016) estimated their model parameters using the experimental work of Safaa (2009). The specification of the experimental apparatus and the characterization of the catalyst used in their work is presented in Table 1 for the convenience of the readers. The model

parameters are the reaction orders of phenol concentration (n), oxygen partial pressure (m), activation energy (EA) and pre-exponential factor (A^0). Their values as reported by Mohammed *et al.* (2016) are 2.1066 (-), 0.6112 (-), 16315.735 $\left(\frac{J}{mol}\right)$ and 668879.2 $(s^{-1}(\frac{cm^3}{mol})^{-1.11})$ respectively.

Table 1. Specification of experimental apparatus and the membrane used in CWAO process and RO process (Safaa, 2009; Srinivasan *et al*., 2010)

Parameter	Value
Length of reactor	77 cm
Length of bed catalyst (L_r)	30 cm
Inner reactor diameter (D_r)	1.9 cm
Volume of catalyst in bed (V_{cat})	85 cm³
Construction material	Stainless steel
Catalyst (Pt/ɣ–Al2O3):	
Particle shape	Sphere
Active phase	(0.48 wt%) Pt
Support	ɣ–Al2O3
Calcination temperature	400 °C
Bulk density (ρ_{cat})	0.647 (g/cm³)
Pore volume (V_g)	0.308 (cm³/g)
Specific surface area of particle (S_g)	259.9 (m²/g)
Particle diameter (d_{pe})	1.6 (mm)
Membrane:	
Supplier	Ion Exchange, India
Membrane material and module configuration	TFC Polyamide, spiral wound
Feed spacer thickness (t_f)	0.85 mm
Effective membrane area (A)	0.75 m²
Module width (W)	1.6667 m
Module length (L)	0.45 m
Module diameter	0.0635 m

3.3.2 RO Process

Murthy and Gupta (1999) used a nonlinear parameter estimation technique of Box-Kanemasu method, which showed that the model parameters of sodium cyanide separation with thin film composite polyamide membrane are nearly constant over the operating conditions. Therefore, it is important to investigate the impact of operating parameters on the model transport parameters. The experimental data of Srinivasan *et al.* (2010) (reported in Section 4.2) have been used to predict the best values of the required unknown parameters of the model. The model is then used to compare model prediction results with experimental data of phenol rejection under different operating conditions. The characteristics of the spiral-wound module are presented in Table 1.

The unknown parameters of the proposed model are the water permeability constant A_w, the phenol permeability constant B_s and the friction parameter b.

The parameter estimation problem can be formulated as follows:

Given: Inlet feed concentration $C_{s(0)}$, inlet flow rate $F_{b(0)}$, inlet feed pressure $P_{b(0)}$ and operating temperature T_{RO}, Average permeate concentration $C_{p(av)}$, outlet feed flow rate $F_{b(L)}$, outlet feed pressure $P_{b(L)}$, total permeated flow rate $F_{p(Total)}$ and phenol rejection Rej_{RO}.

Obtain: A_w, B_s and b.

Minimise: The sum of square errors (*SSE*).

Subject to: Process model, Process constraints.

SSE for the outlet solute concentration is:

$$SSE = \sum_{i=1}^{N_{Data}} \left[F_{b(L)}^{Exp.} - F_{b(L)}^{Cal.}\right]^2 \quad (1)$$

In Eq. (1), N_{Data}, $F_{b(L)}^{Exp.}$ and $F_{b(L)}^{Cal.}$ are the numbers of test runs, experimental and calculated outlet feed flow rate respectively.

The parameter estimation problem can therefore be mathematically presented as follows:

The complete specification of a parameter estimation problem requires:

Min *SSE*

A_w, B_s, b

Subject to: Equality constraints:

Process Model: $f(z, x(z), \dot{x}(z), u(z), v) = 0$; [0, L]

Inequality constraints:

$$A_w{}^L \leq A_w \leq A_w{}^U$$
$$B_s{}^L \leq B_s \leq B_s{}^U$$
$$b^L \leq b \leq b^U$$

L and U are the lower and upper bounds. A simulation step of the model solver starts the parameter estimation approach by converging the equality constraints (described by f) to satisfy the bounds of inequality constraints of decision variables (A_w, B_s and b). The problem can then be solved by renewing the decision variables in a way, which satisfies the equality and inequality constraints (Mujtaba. 2004).

f(z, x(z), $\bar{x}$(z), u(z), v) = 0; represents the RO process model (Table A.2 in Appendix A) in a compact form. Where, z is the independent variable (length of the reactor or membrane), x(z) is the set of all differential and algebraic variables, $\bar{x}$(z) represents the derivative of x(z) with respect to the length of the reactor or membrane, u(z) is the control variables and v denotes the constant parameters of each process. The reactor or membrane lengths under consideration [0, L] and function f are assumed to be continuously differentiable with respect to all their arguments.

The parameter estimation results are given in Table 2 and show a small variation of transport parameters with the inlet operating conditions of five sets of phenol concentration experiments. Table 3 shows the parameter estimation at a specific feed pressure of 14.8 atm, which is used for the remainder of this work for the simulation of RO process in the hybrid system of TBR-RO (Table 5).

4. Model Validation

4.1 TBR Process

Mohammed *et al.* (2016) validated the TBR process model using the experimental data of Safaa (2009). For the convenience of the reader, Fig. 2 shows the model validation by comparing the phenol rejection experimental results with the model predictions for three cases of reaction temperatures (T). The model predictions are in a full agreement with the experimental data, and readily confirm the robustness of the proposed model.

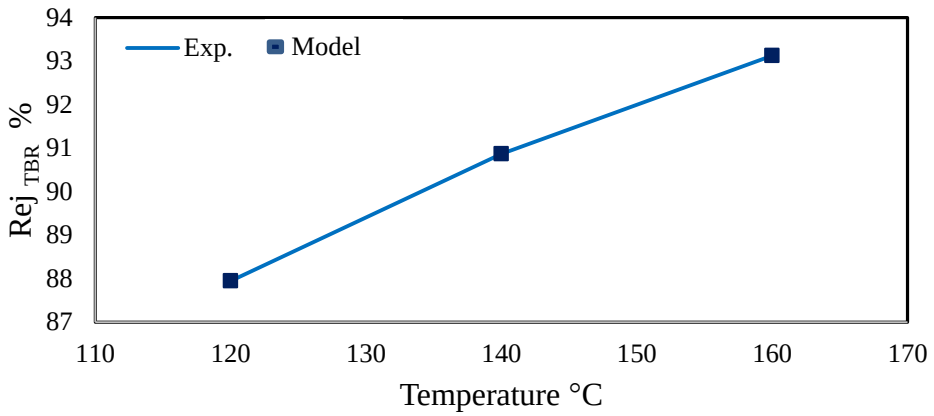

Fig. 2: Experimental and model prediction results of phenol rejection of CWAO process (as per operating conditions given in Section 2.2). Adopted from (Mohammed *et al.*, 2016)

Note, Mohammed *et al.* (2016) showed that the rejection of phenol is between 60 and 94 %, depending on the operating conditions described below:

- Reaction temperature (T): 120, 140 and 160 °C.
- Oxygen partial pressure (P): 7.895, 9.869 and 11.843 atm.
- Liquid hourly space velocity ($LHSV$): 1, 2 and 3 h^{-1}. For 85 cm^3 of catalyst volume, corresponding volumetric wastewater flow rates are 0.000085, 00017 and 0.000255 m^3/h.
- Initial phenol concentration ($C_{ph,L(in)}$): 1000, 3000 and 5000 ppm.
- Gas flow rates (-): 20, 40, 80 and 100 %. Note, such gas flow rate ratio is a stoichiometric excess and it can be used to estimate the gas flow rate or gas velocity from liquid flow rate or liquid velocity. On the other hand, when such ration is 100 %, it means that the gas velocity equals to liquid velocity and when 20 %, means the gas velocity = 0.2 x liquid velocity.

Note that Mohammed *et al.* (2016) are within the operating conditions of Safaa (2009).

4.2 RO Process

In this work, the model of Al-Obaidi *et al.* (2017b) is validated with the experimental data of Srinivasan *et al.* (2010). Srinivasan *et al.* (2010) have used a laboratory-scale RO filtration system consisting of a one commercial thin film composite membrane packed into a spiral

wound polyamide reverse osmosis (RO) module (0.75 m²) for the removal of phenol from its aqueous solutions based on the operating conditions as follows:

- Initial phenol concentration ($C_{b(0)}$): 199.98, 399.97, 599.95, 799.94 and 997.58 ppm.
- Inlet feed flow rate ($F_{b(0)}$): 1.199 m³/h.
- Inlet feed pressure ($P_{b(0)}$): 4.93, 6.9, 8.9, 10.9, 12.8 and 14.8 atm.
- The operating temperature (T_{RO}): 31.5 – 34.5 °C.

The experimental results of Srinivasan *et al.* (2010) confirmed a range of phenol rejection rate of 64 to 87%.

The estimated model parameters values as shown in Table 2. Fig. 3 depicts the comparison of phenol rejection between the experimental results and the model predictions for five sets of inlet feed concentration and pressure (shown in Table 2). Fig. 3 clearly shows that the predicted values of the model are in a good agreement with experimental data.

5. Simulation of the Hybrid TBR-RO Process

In this work, the RO process is kept within the specific operational limits of feed flow rate, pressure and temperature as recommended by the manufacturer. As discussed in section 4, while Srinivasan *et al* (2010) used a feed flow rate of 1.199 m³/h for their RO experimental process Safaa (2009) used a feed flow rate of 0.000051 – 0.000152 m³/h in their experimental study which is significantly lower. In this work we have used wastewater flowrate of 0.58 – 1.74 m³/h. The RO model in this work is validated with a flowrate of 1.199 m³/h and we assume that the model can be used for simulation with flowrate varying from 0.58-1.74 m³/h (1.199 being around the mid-point). However, as the experimental flowrate of TBR is significantly lower, we have considered scaling up the TBR to an acceptable size for a wastewater flow rate of 1.16 m³/h (again being around the middle of 0.58 – 1.199). The TBR scale-up is described below.

Table 2. Parameter estimation results for the RO process

No.	$C_{b(0)}$ (ppm)	$P_{b(0)}$(atm)	T_{RO}(°C)	A_w (m/atm s)	B_s (m/s)	b (atm s/m^4)
1	199.98	4.93	32.5	1.578e-6	2.049e-6	13010.4
2	199.98	6.90	33.1	1.406e-6	1.830e-6	13042.6
3	199.98	8.90	33.0	1.394e-6	1.827e-6	13486.9
4	199.98	10.9	33.2	1.444e-6	1.708e-6	13536.4
5	199.98	14.8	34.0	1.274e-6	1.047e-6	12909.7
6	399.97	4.93	32.2	1.508e-6	1.251e-6	13005.3
7	399.97	6.90	32.8	1.371e-6	1.346e-6	13038.3
8	399.97	8.90	33.5	1.375e-6	7.977e-7	13482.6
9	399.97	10.9	33.9	1.293e-6	1.055e-6	13513.0
10	399.97	12.8	34.5	1.280e-6	1.034e-6	12871.3
11	399.97	14.8	34.5	1.293e-6	1.091e-6	12910.7
12	599.96	4.93	32.5	1.498e-6	8.352e-7	13003.3
13	599.96	6.90	33.0	1.205e-6	9.110e-7	13024.3
14	599.96	8.90	33.2	1.175e-6	1.021e-6	13459.9
15	599.96	10.9	33.5	1.073e-6	8.414e-7	13481.2
16	599.96	12.8	33.8	1.095e-6	8.219e-7	12840.2
17	599.96	14.8	34.0	1.184e-6	5.880e-7	12887.5
18	799.94	4.93	32.0	1.482e-6	1.289e-6	13001.7
19	799.94	6.90	32.5	1.273e-6	1.365e-6	13028.6
20	799.94	8.90	32.8	1.240e-6	1.347e-6	13465.5
21	799.94	10.9	33.0	1.273e-6	1.176e-6	13506.7
22	799.94	12.8	33.2	1.183e-6	1.092e-6	12852.2
23	799.94	14.8	33.5	1.238e-6	1.045e-6	12895.6
24	997.58	4.93	31.5	1.283e-6	1.067e-6	12991.7
25	997.58	6.90	32.2	1.176e-6	1.142e-6	13020.2
26	997.58	8.90	32.6	1.187e-6	1.052e-6	13458.3
27	997.58	10.9	32.8	1.175e-6	1.031e-6	13491.8
28	997.58	12.8	32.8	1.156e-6	9.814e-7	12846.2
29	997.58	14.8	33.0	1.139e-6	8.030e-7	12875.5

Inlet feed flow rate $F_{b(0)}$= 1.1988 m³/h

Table 3. Values of parameter estimation of RO process at a case of 14.8 atm

Parameter	Symbol	Unit	Value
Water permeability coefficient	A_w	(m/s atm)	1.1509E-6
Phenol permeability constant	B_s	(m/s)	8.0434E-7
Friction parameter	b	(atm s/m^4)	12883.0

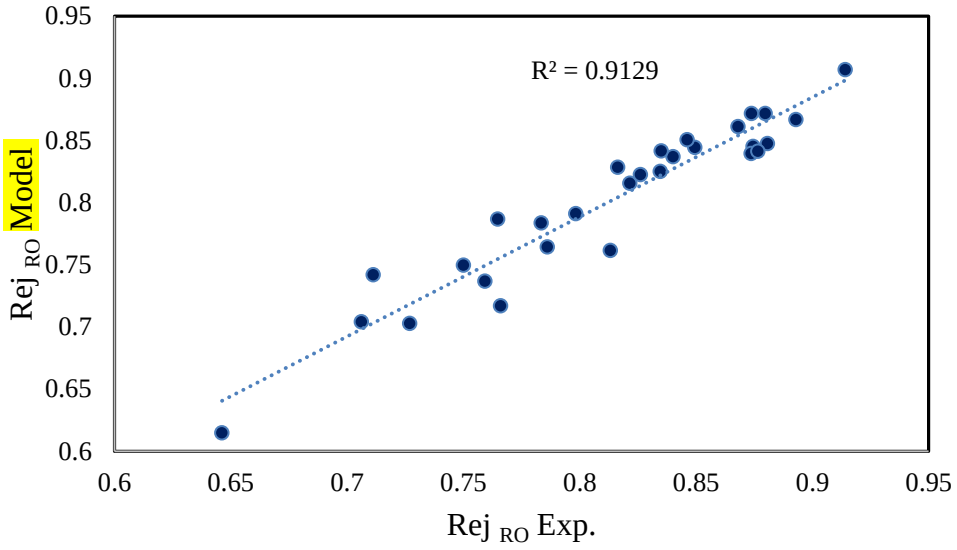

Fig. 3: Experimental and model prediction of phenol rejection of RO process (inlet conditions mentioned in Section 2.2)

5.1 Scaling-up TBR Process

In a scale-up procedure as part of the structural design of a large-scale system, the results of the associated experimental small-scale system, require an accurate impact analysis of the operational conditions on the system. Mohammed *et al.* (2016) presented the TBR laboratory scale-up requirements; i.e. a catalyst volume of 85 cm³ into an industrial scale of catalyst volume of 52 m³ for a wastewater flow of 15-45 m³/h (significantly larger than the flow rate considered in this study). This has been achieved by implementing an energy balance model in trickle bed reactor to represent the non-isothermal state of such size. The ratio of reactor dimensions of bed length (L_r) and inner diameter (D_r) of the reactor were optimised while meeting the hydrodynamic conditions (Bischoff and Levenspiel, 1962) of the large-scale reactor same as the lab scale reactor as described below.

$$\frac{L_r}{D_r} > 0.04 \frac{u_l D_r}{\varepsilon_1 D_r^L} \quad (1)$$

u_l, ε_1 and D_r^L are superficial liquid velocity (cm/s), the liquid phase fraction (-) and the radial mass dispersion coefficient (cm²/s) respectively. For a 52 m³ of active reactor bed, the optimum length and diameter of the reactor were reported to be 9.23 m and 2.69 m respectively.

We have adopted the same principal for the scale-up and the ratio of bed length (L_r) and inner reactor diameter (D_r) and the specific dimensions of the TBR are given in Table 4. Eqs. (26), (27) and (32) given in Table A.1 of Appendix A, are used to estimate the new bed porosity (ε_B), particle density (ρ_p) and catalyst particle porosity (ε_s) of the scaled up TBR. The values of these parameters are also given in Table 4.

Table 4. Specifications of scaled-up trickle bed reactor

Parameter	Value
Length of reactor (L_r)	3.20 (m)
Inner reactor diameter (D_r)	0.72 (m)
Volume of reactor	1.3 (m^3)
Length of bed catalyst (Z)	2.46 (m)
Ration of $\frac{L_r}{D_r}$	3.43 (-)
Volume of catalyst in bed (V_{cat})	1 (m^3)
The bed porosity (ε_B)	0.5253 (-)
The particle density (ρ_p)	1.363 (g/cm^3)
The catalyst particle porosity (ε_s)	0.4198 (-)

The above scale-up procedure uses the same operating conditions of Mohammed *et al.* (2016) in respect of the initial phenol concentration, reaction temperature, liquid hourly space velocity, oxygen partial pressure and gas flow rate.

It is noteworthy to mention that the idea behind using a hybrid TBR-RO system is that the TBR effluent still contains a significant amount of phenol, and a further treatment is required before discharging or save it as reused water. Therefore, the RO process can be integrated with the TBR process as an efficient hybrid technology for reducing phenol concentration. Note the inlet feed temperature and feed pressure for the RO process are 34 °C and 14.8 atm respectively.

6. Results and Discussion

For a range of wastewater flow rate, phenol concentration, oxygen partial pressure and reaction temperature, Table 5 presents the results of TBR and RO processes and the hybrid TBR-RO system. The phenol rejection rate is found to be in the range of 95.384–99.145 %. The integrated TBR-RO process enhances the rejection of TBR process by 4– 55%.

The cases 1 to 9 in Table 5 of the TBR process confirm that for a given inlet feed flow rate, inlet phenol concentration and oxygen partial pressure, an increase of the reaction temperature enhances the phenol rejection. This is due to the directly proportional relation between the reaction rate and reaction temperature and the inversely proportional relation between the reaction rate and activation energy (Eq. (8) in Table A.1). This trend is in-line with Safaa (2009) and confirms the validity of the scaled-up TBR (from 85 cm^3 to 1 m^3). However, it is observed that any increase in the inlet feed flow rate at constant inlet phenol concentration, reaction temperature and oxygen partial pressure causes a decrease in phenol rejection of the TBR process. This is partly due to the length of time the solution is inside the reactor (residence time). The residence time decreases when the inlet feed flow rate increases, which in turn reduces the rejection of phenol. This trend is again in-line with the observation of Safaa (2009) and again confirms the validity of the scaled-up TBR considered in this work.

The cases 10-12 in Table 5 of the TBR process show that for a given inlet feed flow rate, inlet phenol concentration and temperature, an increase of the oxygen partial pressure slightly increases the phenol rejection. The reason for this can be attributed to an increase in the density and solubility of the gas as the applied oxygen partial pressure is increased. Safaa (2009) also observed similar trend in their lab scale TBR.

The impact of the inlet feed phenol concentration is analysed at constant reaction temperature, oxygen partial pressure, inlet feed flow rate and gas flow rate in the cases13 to 15 of Table 5. It is observed that for a change of phenol concentration from 1000 ppm to 3000 ppm, the rejection of phenol improves by 11% but for a change of phenol concentration from 3000 ppm to 5000 ppm, the rejection of phenol improves by only 2.5%. Increasing the inlet phenol concentration can increase the rejection parameter (perhaps up to a certain value) due to an increase of the phenol molecules covering the active site of the catalyst. This phenomenon (with similar trend) is also reported in the experimental work of Safaa (2009). For a given inlet feed flow rate, inlet phenol concentration, temperature and oxygen partial pressure Cases 16 to 27 of Table 5 show the insignificant impact of the gas flow rate on phenol rejection.

Rejection of organic compounds by the RO process is affected by the operating conditions of the inlet feed solution, membrane type, solute, molecular weight and width and the electrostatic interaction between the matrix of the membrane and the solute, which controls the sorption or desorption of the solute (Murthy and Gupta, 1998; Verliefde *et al.*, 2008). According to the

results of Table 5, the wastewater feed flowrate to TBR and RO varies from 0.58 – 1.199 m^3/h and the phenol concentration at the TBR outlet varies from 185 to 1940 ppm. Note that RO model developed in this work is validated against the experimental data of Srinivasan *et al.* (2010) where the feed flow rate was 1.199 m^3/h and the inlet phenol concentration was varied between 200-1000 ppm. Although the predictions of the scaled-up TBR could be justified against the trend observed in experimental lab scale TBR, the predictions by the RO model as presented in Table 5 could not be verified (although we assume that the predictions by the validated model will be accurate) against the experimental data of Srinivasan *et al.* (2010). Therefore, we resort to comparing the trends against observations in the literature for similar situations.

Table 5 shows that phenol rejection increases only slightly due to an increase in the inlet phenol concentration or feed flow rate albeit at constant values of the other operating variables. Li *et al.* (2010) confirmed that the feed concentration and flow rate have little impact on phenol rejection. This in turn confirms the findings of this research. However, Table 5 shows that the simultaneous increase of feed concentration and flow rate can cause a significant increase in phenol rejection. This is due to the increase in the membrane solute isolation intensity, as a result of the underlying increase of the feed concentration and the resulting reduction of the concentration polarization impact due to increasing the feed flow rate. Moreover, it can be argued that increasing the feed concentration causes an increase in the phenol flux through the membrane, but the associated increase of phenol concentration at the permeate channel is incomparable with the increase of phenol concentration at the feed channel. Therefore, the phenol rejection is according to Eq. (18) in Table A.2 of Appendix A. Similar results have been confirmed by Gómez *et al.* (2009) for three types of tested membranes.

The results shown in Table 5 clearly show that the hybrid TBR-RO system was more effective in respect of the treatment efficiency. The combined system can achieve higher separation performance of high phenol concentration from wastewater compared with single processes used in isolation. With inlet phenol concentration of 5000 ppm, the hybrid TBR-RO process can reduce the concentration to 42 ppm (highest being 230 ppm) rejecting more than 99% of the phenol. It must be stressed that the proposed hybrid TBR-RO system has not been used in practice yet and remain therefore theoretical at this stage.

The proposed hybrid TBR-RO system can be made more efficient by adopting the following:

1. The retentate stream of the RO process can be used to reduce the energy consumption of the integrated process taking advantage of the energy recovery device.
2. The use of heat recovered from the hot stream of the heat exchanger to heat up the feed stream of reactor and reduce the total energy consumption provides a highly economical and sustainable solution.
3. Higher feed temperature for RO can increase the permeate recovery.
4. The retentate stream of the RO process can be recycled back to the feed stream of the reactor for further rejection of phenol.

Table 5. Results of TBR process and RO process and hybrid TBR-RO system

	TBR process						RO process				TBR-RO integrated process	
Case	Inlet feed flow rate (m^3/h)	Inlet phenol concentration (ppm)	Reaction temperature (°C)	Oxygen partial pressure (atm)	Gas flowrate (%)	% Phenol rejection (-)	Inlet feed concentration (ppm)	Inlet feed flowrate (m^3/h)	Permeate concentration (ppm)	% Phenol rejection (-)	% Phenol rejection (-)	% Benefit
1	0.58	5000	120	7.895	80	88.720	563.96	0.58	96.42	82.902	98.071	10.54
2	0.58	5000	140	7.895	80	91.039	448.05	0.58	76.77	82.865	98.464	8.15
3	0.58	5000	160	7.895	80	93.330	333.47	0.58	57.26	82.826	98.854	5.92
4	1.16	5000	120	7.895	80	74.788	1260.56	1.16	166.15	86.818	96.676	29.26
5	1.16	5000	140	7.895	80	79.705	1014.72	1.16	133.72	86.821	97.325	22.10
6	1.16	5000	160	7.895	80	84.454	777.25	1.16	102.41	86.823	97.951	15.98
7	1.74	5000	120	7.895	80	61.189	1940.52	1.74	230.78	88.106	**95.384**	**55.88**
8	1.74	5000	140	7.895	80	67.433	1628.32	1.74	193.19	88.135	96.136	42.56
9	1.74	5000	160	7.895	80	73.643	1317.80	1.74	155.99	88.162	96.880	31.55
10	0.58	5000	160	7.895	80	93.330	333.47	0.58	57.26	82.826	98.854	5.92
11	0.58	5000	160	9.869	80	94.349	282.52	0.58	48.56	82.800	99.028	4.96
12	0.58	5000	160	11.843	80	94.780	260.95	0.58	44.88	82.801	99.102	4.56
13	0.58	1000	160	11.843	80	81.456	185.43	0.58	31.94	82.774	96.805	18.84
14	0.58	3000	160	11.843	80	92.580	222.57	0.58	38.31	82.787	98.722	6.63
15	0.58	5000	160	11.843	80	95.035	248.24	0.58	42.70	82.796	**99.145**	4.32
16	0.58	5000	140	7.895	20	91.038	448.07	0.58	76.77	82.865	98.464	8.15
17	1.16	5000	140	7.895	20	79.704	1014.76	1.16	133.72	86.821	97.325	22.10
18	1.74	5000	140	7.895	20	67.432	1628.35	1.74	193.19	88.135	96.136	42.56
19	0.58	5000	140	7.895	40	91.038	448.06	0.58	76.77	82.865	98.464	8.156

20	1.16	5000	140	7.895	40	79.705	1014.74	1.16	133.72	86.821	97.325	22.10
21	1.74	5000	140	7.895	40	67.433	1628.34	1.74	193.19	88.135	96.136	42.56
22	0.58	5000	140	7.895	80	91.039	448.05	0.58	76.77	82.865	98.464	8.15
23	1.16	5000	140	7.895	80	79.705	1014.72	1.16	133.72	86.821	97.325	22.10
24	1.74	5000	140	7.895	80	67.433	1628.32	1.74	193.19	88.135	96.136	42.56
25	0.58	5000	140	7.895	100	91.039	448.05	0.58	76.77	82.865	98.464	8.15
26	1.16	5000	140	7.895	100	79.705	1014.72	1.16	133.72	86.821	97.325	22.10
27	1.74	5000	140	7.895	100	67.433	1628.31	1.74	193.18	88.135	96.136	42.56

Inlet feed pressure $P_{b(0)}$and temperature $T_{RO}$of RO process = 14.8 atm and 34℃.

7. Conclusions

This work has presented a hybrid trickle bed reactor (TBR) and reverse osmosis (RO) process for the removal of phenol from wastewater. Model based approach has been considered to evaluate the effectiveness of the hybrid process. The models of the individual constituent of the hybrid process have been validated against laboratory scale experimental data and in doing so unknown parameters of the models are evaluated. Optimisation based scaling up technique has been implemented for the TBR process to allow feed flow rate of the TBR to be consistent with the feed flow rate of the RO process.

The results of the research confirm that the proposed methodology is both valid and feasible to reject phenol from wastewater at a very high rate.

The research has also demonstrated that the combined use of TBR with RO as a hybrid treatment system can produce high quality water from impaired wastewater streams for re-use. The results of the various cases studied confirm that the combined approach yields a higher phenol rejection from wastewater than the reaction or separation processes used in isolation. The results show that the RO process can increase the phenol removal of pilot-scale TBR process with a range of 4.32 – 55.88 % taking into consideration the inlet operating conditions of the TBR process.

Despite significant progress has been made in this research which has yielded an even greater phenol rejection from wastewater, but there is still room for improvement for achieving a better and cheaper solution. This would require testing different capacities of pilot and industrial plants and implementing superstructure optimisation and multistage RO process. Also, it would be interesting to investigate the advantages of recycling the retentate stream of RO process to TBR process. This in turn can enhance the rejection of other hazardous organic compounds such as N-nitrosamine.

Nomenclature

A : Effective membrane area of the RO process (m^2).

A_w: Solvent transport coefficient of the membrane of the RO process (m/atm s).

A^0 : Pre-exponential factor of the TBR process $(mol/cm^3)^{1-n}\ s^{-1}$).

a_{GL} : Specific gas-liquid contact area per unit volume of bed of the TBR process (cm^{-1}).

a_{LS} : Specific liquid-solid contact area per unit volume of bed of the TBR process (cm^{-1}).

b : Feed and permeate channels friction parameter of the RO process ($atm\ s/m^4$).

B_s : Solute transport coefficient of the RO process (m/s).

$C_{b(x)}$: Phenol concentration in any point along the x-axis of the feed channel of the RO process (kmol/m³).

$C_{b(0)}$: Inlet phenol concentration of the feed channel of the RO process (kmol/m³).

$C_{b(L)}$: Outlet phenol concentration of the feed channel of the RO process (kmol/m³).

C_{O2} : Concentration of oxygen of the TBR process (mol/cm³).

$C_{O2,G}$: Concentration of oxygen in gas phase of the TBR process (mol/cm³).

$C_{O2,L}$: Concentration of oxygen in liquid phase of the TBR process (mol/cm³).

$C_{O2,L-S}$: Concentration of oxygen at liquid-solid interface of the TBR process (mol/cm³).

$C_{p(av)}$: Average permeate phenol concentration in the permeate channel of the RO process (kmol/m³).

$C_{p(0)}$: Inlet permeate phenol concentration of the permeate channel of the RO process (kmol/m³).

$C_{p(L)}$: Outlet permeate phenol concentration of the permeate channel of the RO process (kmol/m³).

C_{ph} : Concentration of phenol of the TBR process (mol/cm³).

$C_{ph,L}$: Concentration of phenol in liquid phase of the TBR process (mol/cm³).

$C_{ph,L(in)}$: Initial phenol concentration of TBR process of the TBR process (ppm).

$C_{ph,L(out)}$: Outlet phenol concentration of TBR process of the TBR process (ppm).

$C_{ph,L-S}$: Concentration of phenol at liquid-solid interface of the TBR process (mol/cm³).

$C_{w(x)}$: Phenol concentration at the membrane wall in any point along the x-axis of the feed channel of the RO process (kmol/m³).

$D_{b(x)}$: Diffusivity parameter of feed in any point along the x-axis of the feed channel of the RO process (m²/s).

D_{ei} : Effective diffusivity of the TBR process (cm²/s).

$D_{kn,i}$: The Knudsen diffusivity of the TBR process (cm²/s).

D_{ph}^{L} : Molecular diffusivity of phenol in liquid phase of the TBR process (cm²/s).

D_{O2}^{L} : Molecular diffusivity of oxygen in liquid phase of the TBR process (cm²/s).

d_p : Diameter of catalyst particle of the TBR process (cm).

d_{pe} : Equivalent diameter particle of catalyst of the TBR process (cm).

D_r : Reactor diameter of the TBR process (cm).

D_r^L : The radial mass dispersion coefficient (cm^2/s).

d_t : Tube diameter of the TBR process (cm).

EA : Activation energy of the TBR process (J/mol K).

$F_{b(x)}$: Feed flow rate in any point along the x-axis of the feed channel of the RO process (m^3/s).

$F_{b(0)}$: Inlet feed flow rate of the feed channel of the RO process (m^3/s).

$F_{p(x)}$: Permeate flow rate in any point along the x-axis of the permeate channel of the RO process (m^3/s).

$F_{p(L)}$: Total Permeated flow rate of the RO process (m^3/s).

H_{O2} : Henry's law constant for dissolved oxygen in water of the TBR process (-).

$J_{s(x)}$: Phenol molar flux in any point along the x-axis of the feed channel of the RO process ($kmol/m^2\ s$).

$J_{w(x)}$: Water flux in any point along the x-axis of the feed channel of the RO process (m/s).

$k_{(x)}$: Mass transfer coefficient in any point along the x-axis of the feed channel of the RO process (m/s).

K_{GL} : Gas-to-liquid mass transfer coefficient of the TBR process (cm/s).

K_{het} : Apparent reaction rate constant of the TBR process $(mol/cm^3)^{1-n}\ s^{-1}$).

K_{LS} : Liquid-to-solid mass transfer coefficient of the TBR process (cm/s).

K_{ph} : Adsorption equilibrium constant of phenol of the TBR process (cm^3/s).

K_{O2}^L : Gas-liquid mass transfer coefficient of the TBR process (cm/s).

kgbw: body weight (kg)

L : Length of the membrane of the RO process (m).

$LHSV$: Liquid hourly space velocity of the TBR process (h^{-1}).

L_r : Bed length of reactor of the TBR process (cm).

n : Order of phenol concentration of the TBR process (-).

m : Order of oxygen partial pressure of the TBR process (-).

MW_{ph} : Molecular weight of phenol (-).

MW_{O2} : Molecular weight of oxygen (-).

P : Partial pressure of oxygen of the TBR process (bar).

$P_{b(x)}$: Feed pressure in any point along the x-axis of the feed channel of the RO process (atm).

$P_{b(0)}$: Inlet feed pressure of the feed channel of the RO process (atm).

P_c : Critical pressure of phenol of the TBR process (psia).

P_p : Permeate pressure at the permeate channel of the RO process (atm).

R : Gas low constant $\left(\mathrm{R} = 0.082\ \frac{\mathrm{atm\ m^3}}{\mathrm{^\circ K\ kmol}}\right)$, $(8.314\ \frac{\mathrm{J}}{\mathrm{mol\ K}})$.

Rec : Water recovery coefficient of the RO process (-).

r_g : Mean pore radius of the TBR process (cm).

Rej_{RO}: Phenol rejection coefficient of the RO process (-).

Rej_{TBR}: Phenol rejection coefficient of TBR process (-).

r_p : Radius of catalyst particle of the TBR process (cm).

R_{ph} : Rate disappearance of phenol per unit volume of catalyst of the TBR process (mol/cm^3_{cat} s).

S_p : Total geometric surface area of catalyst of the TBR process (cm^2).

S_g : Specific surface area of particle of the TBR process (cm^2/g).

T : Reaction temperature of the TBR process (°C).

T_{RO} : Feed temperature of RO process (°C).

T_{br} : Reduced boiling point temperature of the TBR process (-).

T_c : Critical temperature of phenol of the TBR process (K).

t_f : Feed spacer thickness of the RO process (mm).

T_r : Reduced temperature of the TBR process (K).

u_g : Superficial gas velocity of the TBR process (cm/s).

u_l : Superficial liquid velocity of the TBR process (cm/s).

v_c^L : Critical volume of liquid of the TBR process (cm^3/gmol).

v_c^{ph} : Critical volume of phenol of the TBR process (cm^3/gmol).

V_{cat} : Volume of catalyst of the TBR process (cm^3).

V_g : Total pore volume of the TBR process (cm^3/g).

v_L : Molar volume of liquid of the TBR process (cm^3/gmol).

v_{O2} : Molar volume of oxygen of the TBR process (cm^3/gmol).

V_p : Total geometric volume of catalyst particle of the TBR process (cm^3).

W : Width of the membrane of the RO process (m).

x : Length of membrane under consideration of the RO process (m).

Z : Catalyst bed length of the TBR process (cm).

Z_c : Critical compressibility factor of phenol of the TBR process (-).

Z_{O2} : Compressibility factor of oxygen of the TBR process (-).

Greek

η_{LS} : Wetting efficiency of the TBR process (-).

η_0 : Effectiveness factor of the TBR process (-).

ε_B : Bed void fraction (bed porosity) of the TBR process (-).

ε_1 : The liquid phase fraction (-).

ρ_{cat} : Catalyst density of the TBR process (g/cm³).

ρ_{ph} : Density of phenol of the TBR process (g/cm³).

ρ_{O2} : Density of oxygen of the TBR process (g/cm³).

μ_{ph} : Viscosity of phenol of the TBR process (m Pa s).

φ : Thiel modulus of the TBR process (-).

τ : The tortuosity factor of the TBR process (-).

References

Ahmed S., Rasul M. G., Martens W. N., Brown R. and Hashib M. A., 2010. Heterogeneous photocatalytic degradation of phenols in wastewater: A review on current status and developments, *Desalination*, 261, 3-18.

Al-Obaidi M. A., Kara-Zaïtri C., Mujtaba I. M., 2016. Development and validation of N-nitrosamine rejection mathematical model using a spiral-wound reverse osmosis process. *Chemical Engineering Transactions*. 52, 1129-1134.

Al-Obaidi M. A. and Mujtaba I. M., 2016. Steady state and dynamic modeling of spiral wound wastewaterreverse osmosis process. *Computers and Chemical Engineering*, 90, 278-299.

Al-Obaidi M. A., Kara-Zaïtri C. and Mujtaba I. M., 2017a. Wastewater treatment by spiral wound reverse osmosis: Development and validation of a two dimensional process model. *Journal of Cleaner Production*, 140, 1429-1443.

Al-Obaidi M. A., Li Jian-Ping, Kara-Zaïtri C. and Mujtaba I. M., 2017b. Optimisation of reverse osmosis based wastewater treatment system for the removal of chlorophenol using genetic algorithms. *Chemical Engineering Journal*, 316, 91-100.

Al-Obaidi M. A., Kara-Zaïtri C. and Mujtaba I. M., 2017c. Development of a mathematical model for apple juice compounds rejection in a spiral-wound reverse osmosis process. *Journal of Food Engineering*, 192, 111-121.

Al-Obaidi M. A., Kara-Zaïtri C. and Mujtaba I. M., 2017d. Modeling of a spiral-wound reverse osmosis process and parameter estimation. *Desalination and Water Treatment*, 69, 93-101.

Al-Mutaz I. S., Soliman M. A. and Daghthem A. M., 1989. Optimum design for a hybrid desating plant. *Desalination*, 76, 177-187.

Altaee A. and Hilal N., 2015. High recovery rate NF–FO–RO hybrid system for inland brackish water treatment. *Desalination*, 363, 19-25.

Alzahrani S., Mohammad A. W., Hilal N., Abdullah P. and Jaafar O., 2013a. Comparative study of NF and RO membranes in the treatment of produced water—Part I: Assessing water quality. *Desalination*, 315, 18-26.

Alzahrani S., Mohammad A. W., Hilal N., Abdullah P. and Jaafar O., 2013b. Comparative study of NF and RO membranes in the treatment of produced water II: Toxicity removal efficiency. *Desalination*, 315, 27-32.

Al-Zoubi H., Al-Thyabat S. andAl-Khatib L., 2009. A hybrid flotation–membrane process for wastewater treatment: an overview.*Desalination and Water Treatment*, 7, 60-70.

Ang W. L., Mohammad A. W., Hilal N. and Leo C. P., 2015. A review on the applicability of integrated/hybrid membrane processes in water treatment and desalination plants. *Desalination*, 363, 2-18.

Arsuaga J. M., Sotto A., López-Muñoz M. J., and Braeken L., 2011. Influence of type and position of functional groups of phenolic compounds on NF/RO performance. *Journal of Membrane Science*, 372, 380-386.

Awerbuch L., May S., Soo-Hoo R. and Mast vander V., 1989. Hybrid desalting systems. *Desalination*, 76, 189-197.

Bingham E., Cohrssen B., and Powell C. H., 2001. Patty's Toxicology. Vol. 4. 5th ed. New York, N. Y.: John Wiley and Sons. p. 393.

Bischoff K. B. and Levenspiel O., 1962. Fluid dispersion-generalization and comparison of mathematical models-I Generalization of models. *Chemical Engineering Science,* 17, 245-255.

Busca G., Berardinelli S., Resini C. and Arrighi L., 2008. Technologies for the removal of phenol from fluid streams: A short review of recent developments. *Journal of Hazardous Materials,* 160 (2) 265-288.

EFSA, 2013. Scientific opinion on the toxicological evaluation of phenol. EFSA Journal, 11(4), 3189. Available at: http://www.efsa.europa.eu/en/efsajournal/doc/3189.pdf

E1-Sayed E., Ebrahim S., A1-Saffar A. and Abdel-Jawad M., 1998. Pilot study of MSF/RO hybrid systems. *Desalination*, 120, 121-128.

Frederik Schutte C., 2003. The rejection of specific organic compounds by reverse osmosis membranes. *Desalination,*;158, 285-294.

Geraldes V., Anil A., de Pinho M. N. and Duarte E., 2008. Dissolved air flotation of surface water for spiral-wound module nanofiltration pretreatment. *Desalination*, 228, 191-199.

Gogate P. R. and Pandit A. B., 2004. A review of imperative technologies for wastewater treatment II: hybrid methods. *Advances in Environmental Research*, 8, 553-597.

Gómez J., León G., Hidalgo A., Gómez M., Murcia M. and Griñán G., 2009. Application of reverse osmosis to remove aniline from wastewater. *Desalination*, 245, 687-693.

Helal A. M., El-Nashar A. M., Al-Katheeri E. and Al-Malek S., 2003. Optimal design of hybrid RO/MSF desalination plants Part I: Modeling and algorithms. *Desalination*, 154, 43-66.

Hidalgo A. M., Leon G., Gómez M., Murcia M. D. and Gómez E., Gómez J.L.,2011. Behaviour of RO98pHt polyamide membrane in reverse osmosis and low reverse osmosis conditions for phenol removal. *Environ Technol*., 32, 1497-1502.

Kamal L., Schneider W. and Tusel G. F., 1989. Process arrangements for hybrid sea water desalination plants. *Desalination*, 76, 323-335.

Kim K. -Y., Kim H. -S., Kim J., Nam J. -W., Kim J. -M. and Son S., 2009. A hybrid microfiltration–granular activated carbon system for water purification and wastewater reclamation/reuse. *Desalination*, 243, 132-144.

Koroneos C., Dompros A. and Roumbas G., 2007. Renewable energy driven desalination systems modelling. *Journal of Cleaner Production*, 15, 449-464.

Lee C., Chen Y. and Wang G., 2010. A dynamic simulation model of reverse osmosis desalination systems. The 5th International Symposium on Design, Operation and Control of Chemical Processes, PSE ASIA, Singapore.

Li Y., Wei J., Wang C. and Wang W., 2010. Comparison of phenol removal in synthetic wastewater by NF or RO membranes. *Desalination and Water Treatment,* 22, 211-219.

Mohammed A. E., Jarullah A.T., Gheni S. A. and Mujtaba I. M., 2016. Optimal design and operation of an industrial three phase reactor for the oxidation of phenol. *Computers and Chemical Engineering*, 94, 257-271.

Mohammadi S., Kargari A., Sanaeepur H., Abbassian K., Najafi A. and Mofarrah E., 2015. Phenol removal from industrial wastewaters: a short review. *Desalination and Water Treatment*, 53, 2215-2234.

Mozia S., Janus M., Brożek P., Bering S., Tarnowski K., Mazur J. and Morawski A.W., 2016. A system coupling hybrid biological method with UV/O3 oxidation and membrane separation for treatment and reuse of industrial laundry wastewater. *Environ. Sci. Pollut. Res*. 23, 19145-19155.

Mujtaba I. M. 2004. Batch distillation: Design and operation. Imperial College Press, London, UK.

Murthy Z. V. P. and Gupta S. K., 1998. Thin film composite polyamide membrane parameters estimation for phenol-water system by reverse osmosis. *Separation Science and Technology,* 33(16), 2541-2557.

Murthy Z. V. P. and Gupta S. K., 1999. Sodium cyanide separation and parameter estimation for reverse osmosis thin film composite polyamide membrane. *Journal of Membrane Science,* 154, 89-103.

Ozaki H. and Li H., 2002. Rejection of organic compounds by ultra-lowpressure reverse osmosis membrane. *Water Research*, 36, 123-130.

Pimple S., Karikkat S., Devanna M., Yanamadni V., Sah R. and Prasad S. M. R., 2016. Comparison of MBR/RO and UF/RO hybrid systems for the treatment of coke-oven effluents. *Desalination and Water Treatment*, 57, 3002-3010.

Pomiès M., Choubert J. -M., Wisniewski C. and Coquery M., 2013. Modelling of micropollutant removal in biological wastewater treatments: A review. Science of the Total Environment, 443, 733-748.

Process System Enterprise Ltd, 2001. gPROMS Introductory User Guide. Process System Enterprise Ltd., London.

Safaa M., 2009. Catalytic Wet Air Oxidation of Phenolic Compounds in Wastewaterin a Trickle Bed Reactor at High Pressure. MSc. Thesis. University of Tikrit, Iraq.

Srinivasan G., Sundaramoorthy S. and Murthy D. V. R., 2010. Spiral wound reverse osmosis membranes for the recovery of phenol compounds – Experimental and parameter estimation studies. *American Journal of Engineering and Applied Science*, 3(1), 31-36.

Sudilovskiy P., Kagramanov G. and Kolesnikov V., 2008. Use of RO and NF for treatment of copper containing wastewaters in combination with flotation, *Desalination*, 221, 192-201.

Sundaramoorthy S., Srinivasan G. and Murthy D. V. R. 2011a. An analytical model for spiral wound reverse osmosis membrane modules: Part I — Model development and parameter estimation. *Desalination, 280(1-3),* 403-411.

Verliefde A. R. D., Heijman S. G. J., Cornelissen E. R., Amy G. L., Van der Bruggen B., and van Dijk J. C., 2008. Rejection of trace organic pollutants eith high pressure membranes (NF/RO). *Environmental Progress*,27(2), 180-188.

Wankat P. C., 1990. Rate-Controlled Separation. 1st Edn., Springer, ISBN: 10: 1851665218, pp: 87.

Appendix A

Table A.1. Modelling of TBR process (Mohammed *et al.*, 2016)

Model Equations	Specifications	No.
$\frac{dC_{O2,G}}{dZ} = -\left(\frac{K_{GL}\, a_{GL}}{u_g}\right)\left(\frac{C_{O2,G}}{H_{O2}} - C_{O2,L}\right)$	The concentration of oxygen and the mass transfer across the gas–liquid interface.	1
$\frac{dC_{ph,L}}{dZ} = -\left(\frac{\eta_{LS}\, K_{LS}\, a_{LS}}{u_l}\right)\left(C_{ph,L} - C_{ph,L-S}\right)$	The mass balance equations for the concentrations of phenol in the liquid phase.	2
$\frac{dC_{O2,G}}{dZ} = -\left(\frac{K_{GL}\, a_{GL}}{u_l}\right)\left(\frac{C_{O2,G}}{H_{O2}} - C_{O2,L}\right) - \left(\frac{\eta_{L,S}\, K_{L,S}\, a_{L,S}}{u_l}\right)\left(C_{O2,L} - C_{O2,L-S}\right)$	The mass balance equations for the concentrations of oxygen in the liquid phase.	3
$K_{LS}\, a_{LS}\left(C_{ph,L} - C_{ph,L-S}\right) = \eta_0\,(1-\varepsilon_B)\, R_{ph}$	The phenol chemical reaction.	4
$K_{L,S}\, a_{LS}\left(C_{O2,L} - C_{O2,L-S}\right) = 7\eta_0\,(1-\varepsilon_B)\, R_{ph}$	The oxygen chemical reaction.	5
$R_{ph} = \rho_{cat}\, K_{het}\, \frac{C_{ph}^{n}\, C_{O2}^{m}}{\left(1 + K_{ph}\, C_{ph,L}\right)^2}$	The kinetic equation of Langmuir–Hinshelwood type that accounts for phenol disappearance.	6
$K_{ph} = exp\left(-\frac{364.47}{T} - 2.3854\right)$	Calculates the adsorption equilibrium constant of phenol (K_{ph}).	7
$K_{het} = A^0\, exp\left(-\frac{EA}{RT}\right)$	Calculates the Reaction rate constant (K_{het}).	8
$\frac{K_{O2}^{L}\, a_L}{D_{O2}^{L}} = 7\left(\frac{\rho_{ph}\, u_l}{\mu_{ph}}\right)^{0.4}\left(\frac{\mu_{ph}}{\rho_{ph}\, D_{O2}^{L}}\right)^{0.5}$	Calculates the gas–liquid mass transfer coefficient of phenol.	9
$\frac{K_{ph}^{s}}{D_{ph}^{L}\, a_{LS}} = 1.8\left(\frac{\rho_{ph}\, u_l}{a_{LS}\, \mu_{ph}}\right)^{0.5}\left(\frac{\mu_{ph}}{\rho_{ph}\, D_{ph}^{L}}\right)^{1/3}$	Calculates the liquid–solid mass transfer coefficient of phenol.	10
$\frac{K_{O2}^{s}}{D_{O2}^{L}\, a_{LS}} = 1.8\left(\frac{\rho_{ph}\, u_l}{a_{LS}\, \mu_{ph}}\right)^{0.5}\left(\frac{\mu_{ph}}{\rho_{ph}\, D_{O2}^{L}}\right)^{1/3}$	Calculates the liquid–solid mass transfer coefficient of oxygen.	11
$D_{ph}^{L} = 8.93x10^{-8}\, \frac{\nu_L^{0.267}\, T}{\nu_{ph}^{0.267}\, \mu_{ph}}$	Calculates the molecular diffusivity of phenol.	12
$D_{O2}^{L} = 8.93x10^{-8}\, \frac{\nu_L^{0.267}\, T}{\nu_{O2}^{0.267}\, \mu_{ph}}$	Calculates the molecular diffusivity oxygen.	13
$\nu_L = 0.285\,(v_c^{L})^{1.048}$	Calculates The molar volume of liquid (ν_L).	14
$\nu_{ph} = 0.285(v_c^{ph})^{1.048}$	Calculates The molar volume of phenol (ν_{ph}).	15
$\nu_{O2} = 0.285(v_c^{O2})^{1.048}$	Calculates The molar volume of oxygen (ν_{O2}).	16
$H_{O2} = \left(6088.8 - 871.2\ln T - \frac{326284}{T}\right)$	Calculates the Henry's constant for oxygen (H_{O2}).	17
$\rho_{ph} = \frac{MW_{ph}\, P_c}{R\, T_c\, Z_c\, (1-T_r)^{2/7}}$	Calculates the density of phenol.	18
$T_r = \frac{T}{T_c}$	Calculates the reduced temperature.	19
$\rho_{O2} = \frac{P\, MW_{O2}}{Z_{O2}\, R\, T}$	Calculates the density of oxygen.	20
$\mu_{ph} = exp\left(ln(\alpha\, x\, \mu_{ph,b}) x \left(\frac{ln(\mu_{ph,b})}{ln(\alpha\, x\, \mu_{ph,b})}\right)^{\emptyset}\right)$	Calculates the viscosity of phenol.	21
$\emptyset = \frac{1-T_r}{1-T_{br}}$	Calculates the Volume fraction of molecule ($\emptyset$).	22

Table A.1. Modelling of TBR process (Mohammed *et al.*, 2016) (continued)

Model Equations	Specifications	No.
$T_{br}=\frac{T_b}{T_c}$	Calculates the reduced boiling point temperature.	23
$\eta_0 = \frac{3(\varphi\ coth\varphi - 1)}{\varphi^2}$	Calculates the effectiveness factor of for the sphere particle.	24
$\varphi = \frac{V_p}{S_p}\sqrt{\left(\frac{n+1}{2}\right)\left(\frac{K_{het}\ C_{ph}^{n-1}\ \rho_p}{D_{ei}}\right)}$	Calculates the Thiel modulus (φ).	25
$\rho_p = \frac{\rho_{cat}}{1-\varepsilon_B}$	Calculates the particle density (ρ_p).	26
$\varepsilon_B = 0.38 + 0.073\left(1 + \frac{\left(\frac{d_t}{d_{pe}} - 2\right)^2}{\left(\frac{d_t}{d_{pe}}\right)^2}\right)$	Calculates the bed porosity (ε_B).	27
$V_p = \frac{4}{3}\pi(rp)^2$	Calculates the external volume (V_p) of the spherical shape of particle.	28
$S_p = 4\,\pi(rp)^2$	Calculates the surface area (S_p) of the spherical shape of particle.	29
$a_{L,S} = \frac{S_p\ (1-\varepsilon_B)}{V_p}$	Calculates the surface area of particle per unit volume of the bed.	30
$D_{ei} = \frac{\varepsilon_S}{\tau}\frac{1}{\frac{1}{D_{mo.i}} + \frac{1}{D_{kn,i}}}$	Calculates The effective diffusivity (D_{ei}).	31
$\varepsilon_S = \rho_P\ V_g$	Calculates the catalyst particle porosity (ε_S).	32
$D_{kn,i} = 9700\ r_g\sqrt{\frac{T}{MW_{ph}}}$	Calculates the Knudsen diffusivity ($D_{kn,i}$).	33
$r_g = 2\ \frac{V_g}{S_g}$	Calculate the mean pore radius (r_g).	34
$Rej_{TBR} = \frac{C_{ph,L(in)} - C_{ph,L(out)}}{C_{ph,L(in)}}\ x100$	Calculate the rejection of phenol	35

Table A.2. Process model for the spiral-wound RO process (based on Al-Obaidi *et al.*, 2017b but modified for Phenol)

Model Equations	Specifications	No.
$F_{b(x)} = \left\{F_{b(0)} - \left(W\ \theta\ x\ \Delta P_{b(0)}\right) + \left(W\ \theta\ b\ \left(\frac{x^2}{2}\right)\ F_{b(0)}\right) + \left(W\ \theta\ b\ \left(\frac{W\ \theta}{b}\right)^{0.5}\left(\frac{x^2}{2}\right)\ \left(\Delta P_{b(x)} - \Delta P_{b(0)}\right)\right)\right\}$	Calculates feed flow rate at any point along the x-axis.	1
$\theta = \frac{A_w B_s}{B_s + R\ T_{RO}\ A_w\ C_{p(av)}}$	Parameter in Eq. (1).	2
$U_{b(x)} = \frac{F_{b(x)}}{t_f\ W}$	Calculates feed velocity at any point along the x-axis.	3
$P_{b(x)} = \left\{P_{b(0)} - \left(b\ x\ F_{b(0)}\right) + \left(b\ W\theta\ \left(\frac{x^2}{2}\right)\left(\Delta P_{b(x)}\right)\right) - \left[b^2\ W\theta\ \left(\frac{x^3}{6}\right)F_{b(0)}\right] - \left[b^2\ W\ \theta\ \left(\frac{W\ \theta}{b}\right)^{0.5}\left(\frac{x^3}{6}\right)\ \left(\Delta P_{b(x)} - \Delta P_{b(0)}\right)\right]\right\}$	Calculates feed pressure at any point along the x-axis.	4
$\Delta P_{b(x)} = \Delta P_{b(0)} - \left(b\ x\ F_{b(0)}\right) - \left[\left(\frac{W\ \theta}{b}\right)^{0.5} b\ x\ \left(\Delta P_{b(x)} - \Delta P_{b(0)}\right)\right]$	Calculates pressure difference between the feed and permeate channels at any point along the x-axis.	5
$\Delta P_{b(x)} = P_{b(0)} - P_p$	Calculates pressure difference between the feed and permeate channels at x=0.	6
$J_{w(x)} = \theta\ \left\{\left[\Delta P_{b(0)} - \left(b\ x\ F_{b(0)}\right)\right] - \left[\left(\frac{W\ \theta}{b}\right)^{0.5} b\ x\ \left(\Delta P_{b(x)} - \Delta P_{b(0)}\right)\right]\right\}$	Calculates water flux at any point along the x-axis.	7
$J_{s(x)} = B_s\ (C_{w(x)} - C_{p(av)})$	Calculates the solute flux at any point along the x-axis.	8
$\frac{(C_{w(x)} - C_{p(av)})}{(C_{s(x)} - C_{p(av)})} = exp\left(\frac{J_{w(x)}}{k_{(x)}}\right)$	Calculates wall solute concentration at any point along the x-axis.	9
$k_{(x)} = 1.177\ \left(\frac{U_{b(x)}\ D_{b(x)}^2}{t_f\ L}\right)^{0.3333}$	Calculates mass transfer coefficient at any point along the x-axis (Wankat, 1990).	10
$D_{b(x)} = 6.725E-6\ exp\left\{0.1546E-3\ C_{b(x)}\ (18.012) - \frac{2513}{T_{RO}+273.15}\right\}$	Calculates diffusivity parameter at any point along the x-axis (Koroneos, 2007)	11
$\frac{C_{b(x)}}{t_f\ W}\ \frac{dF_{b(x)}}{dx} + \frac{F_{b(x)}}{t_f\ W}\ \frac{dC_{b(x)}}{dx} = \frac{d}{dx}\left[D_{b(x)}\ \frac{dC_{b(x)}}{dx}\right] - \frac{(J_{w(x)}\ C_{p(x)})}{t_f} + \frac{(J_{w(x)}\ C_{b(x)})}{t_f}$	Calculates feed phenol concentration at any point along the x-axis (Lee *et al.*, 2010).	12
$C_{p(av)} = \frac{C_{p(0)} + C_{p(L)}}{2}$	Calculates average permeate solute concentration.	13
$C_{p(0)} = \frac{B_s\ C_{b(0)}\ e^{\frac{J_{w(0)}}{k(0)}}}{J_{w(0)} + B_s\ e^{\frac{J_{w(0)}}{k(0)}}}$ and $C_{p(L)} = \frac{B_s\ C_{b(L)}\ e^{\frac{J_{w(L)}}{k(L)}}}{J_{w(L)} + B_s\ e^{\frac{J_{w(L)}}{k(L)}}}$	Calculates permeate solute concentrations at x=0 and x=L (Al-Obaidi *et al.*, 2017c).	14 15
$F_{p(x)} = F_{p(0)} + \left(W\ x\ \theta\ \Delta P_{b(0)}\right) - \left[W\ \theta\ b\ \left(\frac{x^2}{2}\right)F_{b(0)}\right] - \left[W\ \theta\ b\ \left(\frac{x^2}{2}\right)\left(\frac{W\ \theta}{b}\right)^{0.5}\ \left(\Delta P_{b(x)} - \Delta P_{b(0)}\right)\right]$	Calculates permeated flow rate at any point along the x-axis.	16
$Rec_{(Total)} = \frac{F_{p(L)}}{F_{b(0)}} x\ 100$	Calculates total water recovery.	17
$Rej_{RO} = \frac{C_{b(0)} - C_{p(av)}}{C_{b(0)}} x100$	Calculates solute rejection	18